Electronic Supplementary Material (ESI) for New Journal of Chemistry.


# Self-Assembly of thiolato-bridged ester functionalized Re(I)-based tetranuclear spiro-metallacyclophanes

Jisna Varghese, Udit Kumar, Shilpa Jose, Aamir Afzal Magray, S. Yeswanth Kumar, R. Padmanaban, Bala. Manimaran*

*Department of Chemistry, Pondicherry University, Puducherry, 605014, India*

* Corresponding author. Tel.: +91 413 2654414; fax: +91 413 2656740

E-mail: manimaran.che@pondiuni.edu.in (Bala. Manimaran)

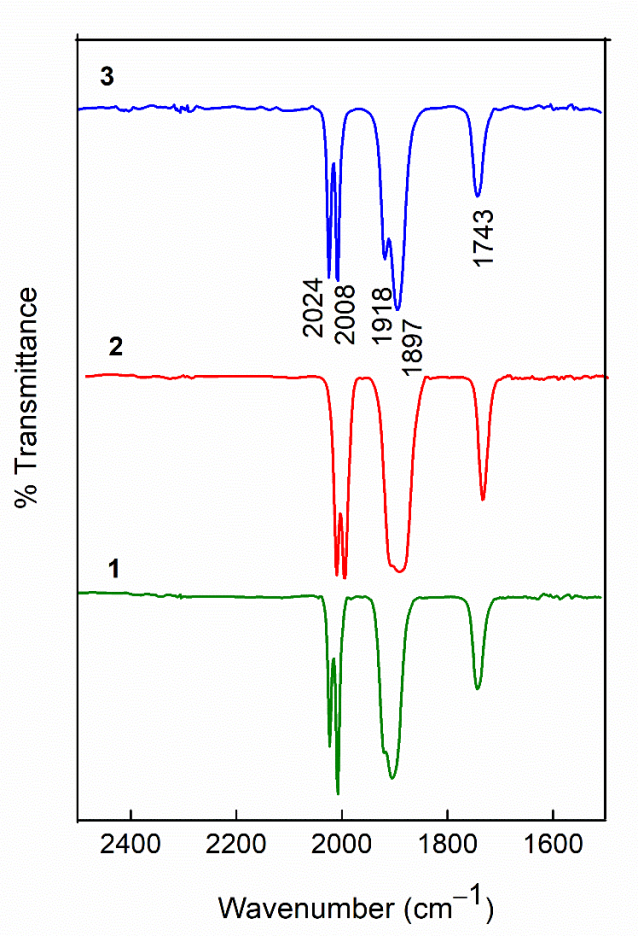


**Fig. S1** Stacked IR spectra of tetranuclear spiro-metallacyclophanes **1–3** in $CH_2Cl_2$.

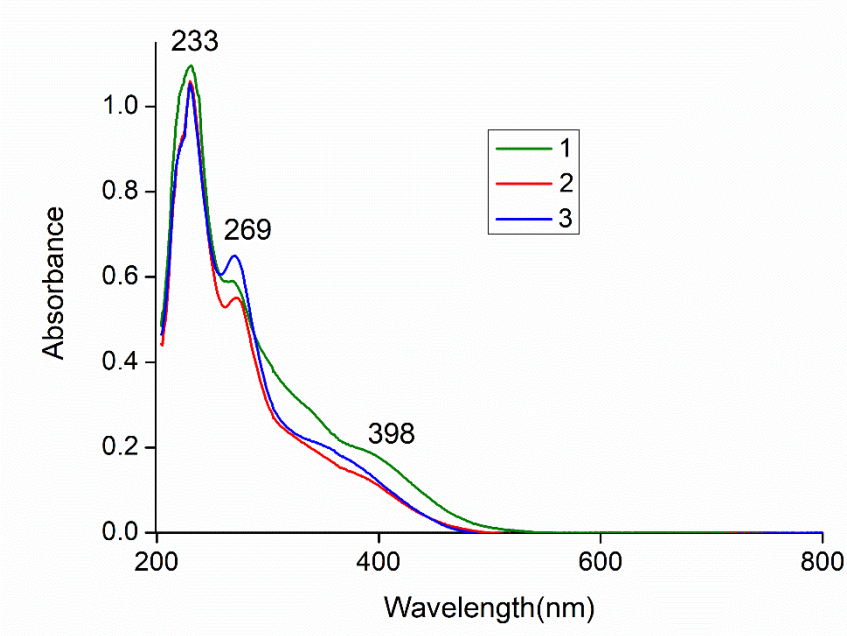


**Fig. S2** Overlay UV–vis absorption spectra of tetranuclear spiro-metallacyclophanes **1–3** in $CH_2Cl_2$.

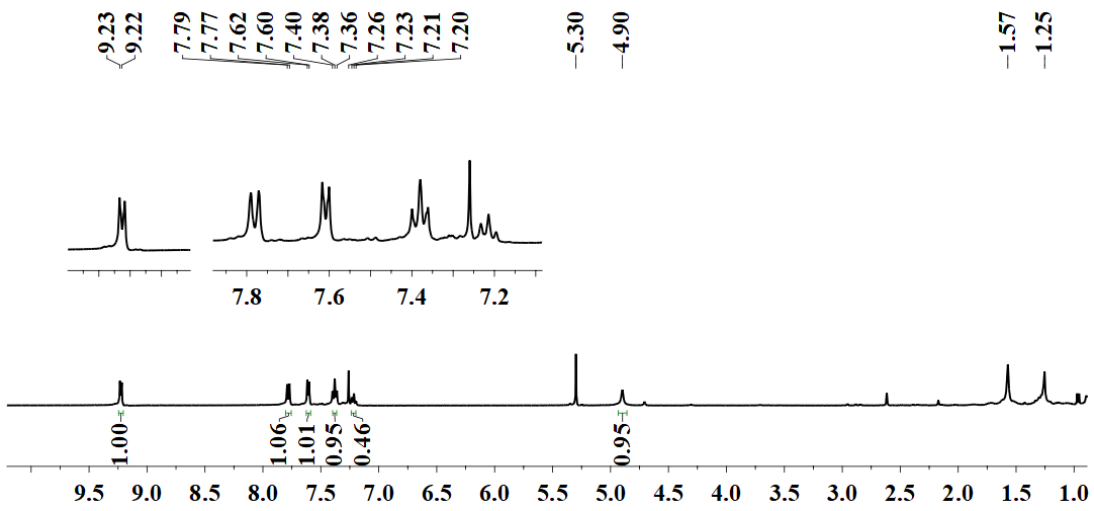


**Fig. S3** $^{1}$H NMR spectrum of [{$(CO)_3Re(\mu\text{-}SC_6H_5)_2Re(CO)_3$}$_2$($\mu$-$\eta^4$-ptpc)] (**1**) in $CDCl_3$.

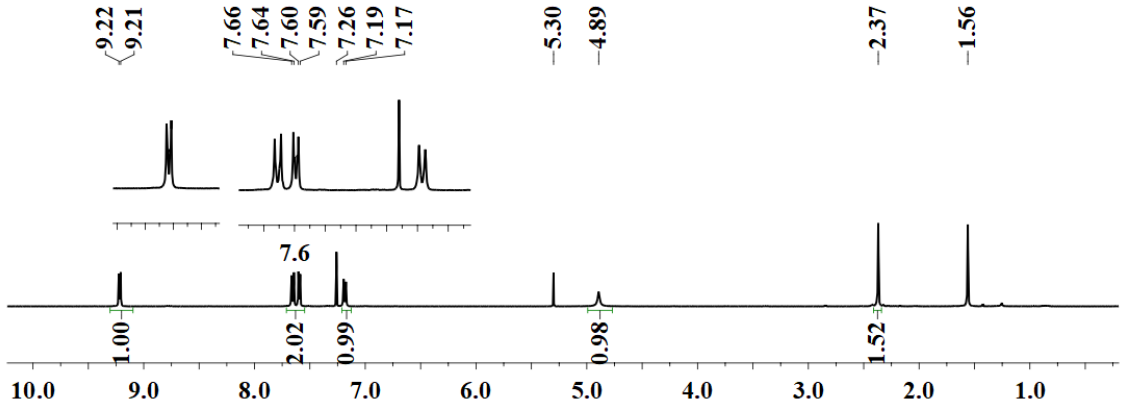


**Fig. S4** $^{1}$H NMR spectrum of [{$(CO)_3Re(\mu\text{-}SC_6H_4CH_3)_2Re(CO)_3$}$_2$($\mu$-$\eta^4$-ptpc)] (**2**) in $CDCl_3$.

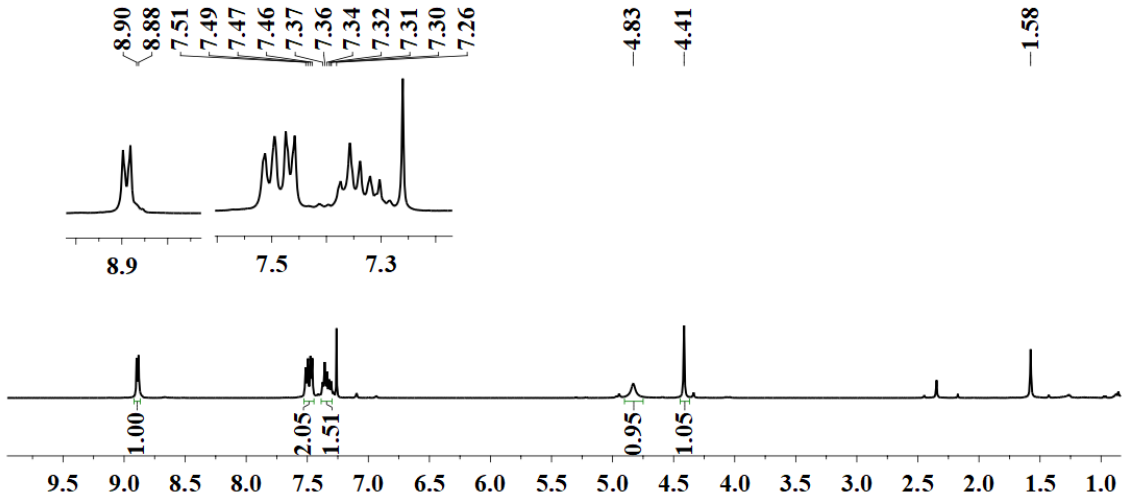


**Fig. S5** $^{1}$H NMR spectrum of [{$(CO)_3Re(\mu\text{-}SCH_2C_6H_5)_2Re(CO)_3$}$_2$($\mu$-$\eta^4$-ptpc)] (**3**) in $CDCl_3$.

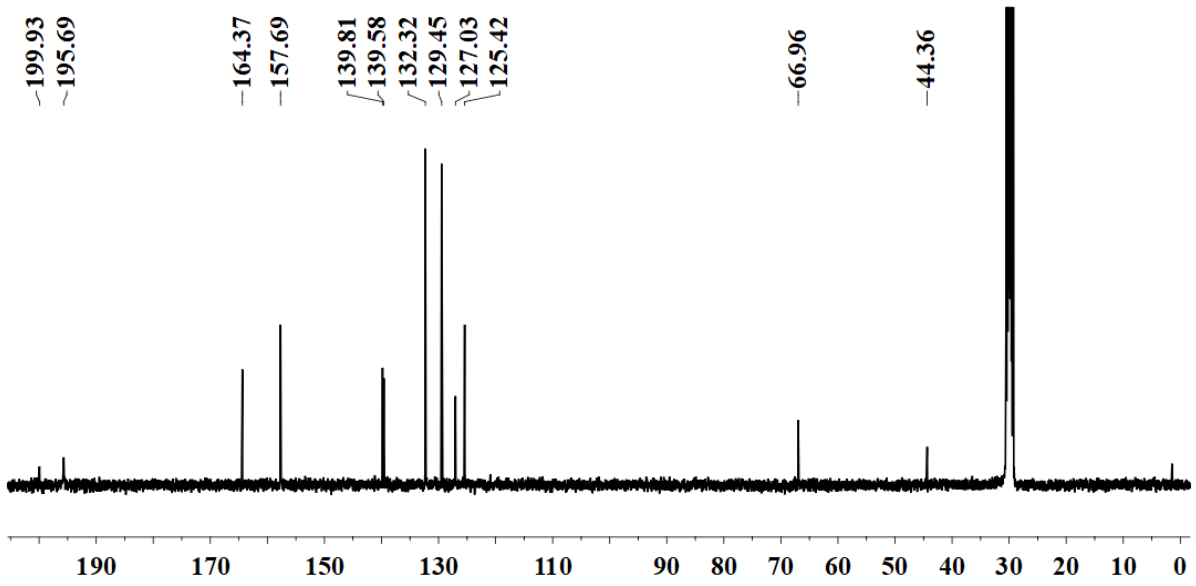


**Fig. S6** $^{13}$C NMR spectrum of [{(CO)$_3$Re($\mu$-SC$_6$H$_5$)$_2$Re(CO)$_3$}$_2$($\mu$-$\eta^4$-ptpc)] (**1**) in $C_3D_6O$.

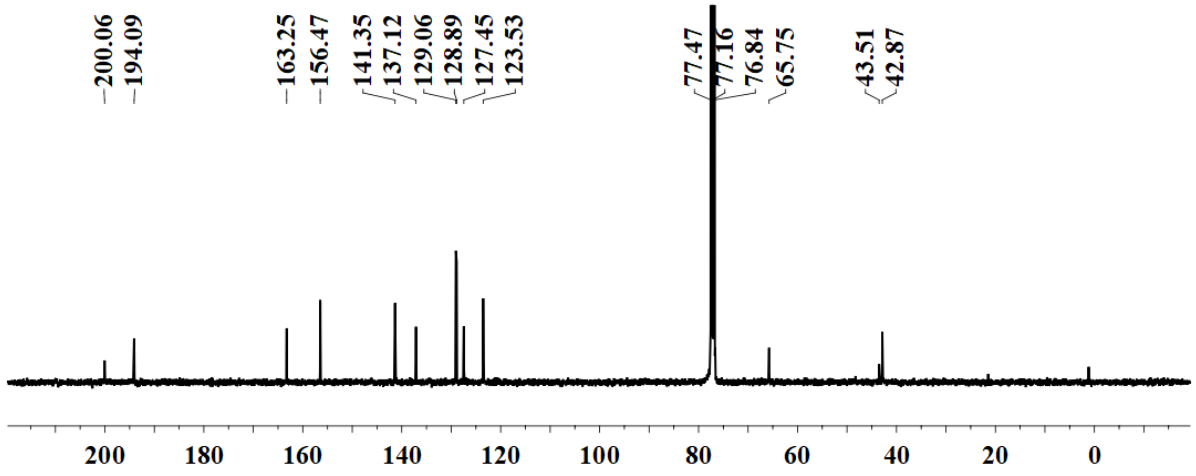


**Fig. S7** $^{13}$C NMR spectrum of [{(CO)$_3$Re($\mu$-SCH$_2$C$_6$H$_5$)$_2$Re(CO)$_3$}$_2$($\mu$-$\eta^4$-ptpc)] (**3**) in $CDCl_3$.

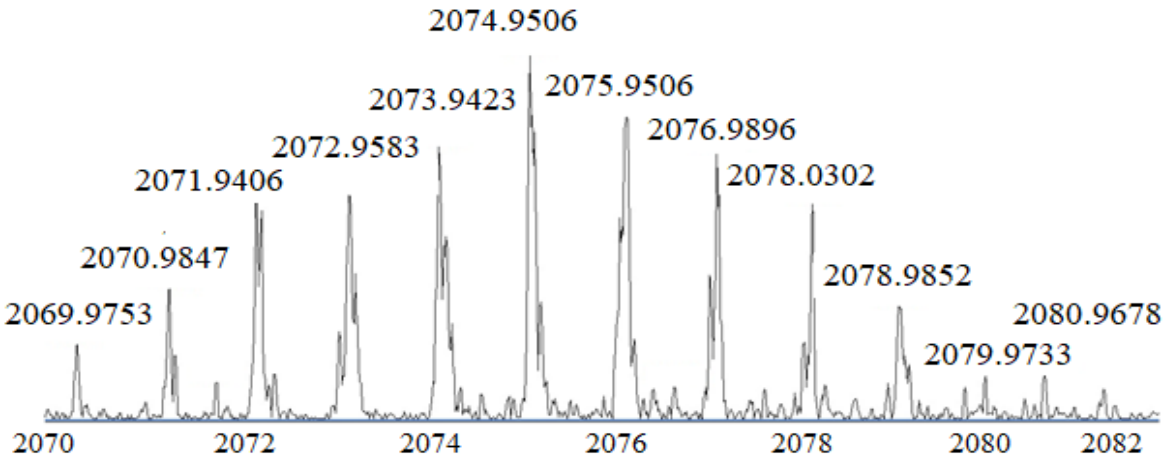


Count *vs* Mass to charge (m/z)

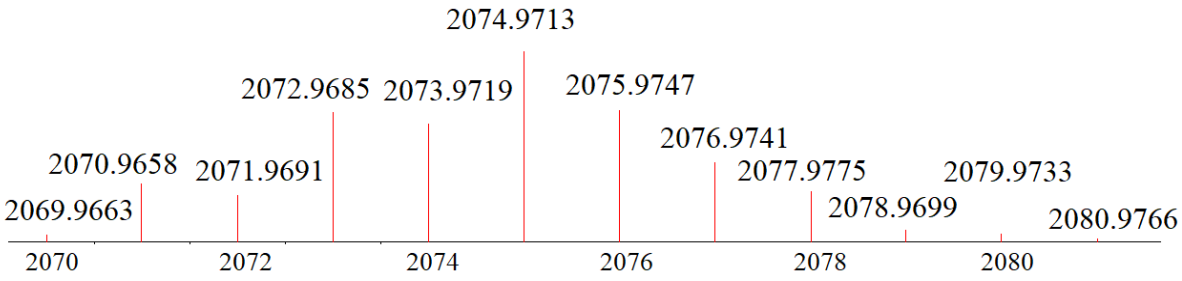


Count *vs* Mass to charge (m/z)

**Fig. S8** Experimental (top) and theoretical (bottom) isotopic distribution patterns of ESI-mass spectrum of [{$(CO)_3Re(\mu\text{-}SC_6H_5)_2Re(CO)_3$}$_2$($\mu$-$\eta^4$-ptpc)] (**1**) $[M]^+$.

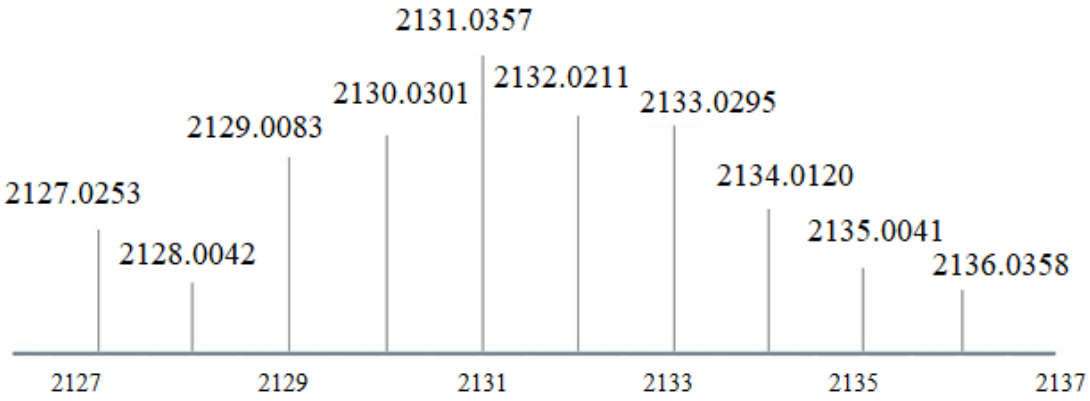


Count *vs* Mass to charge (m/z)

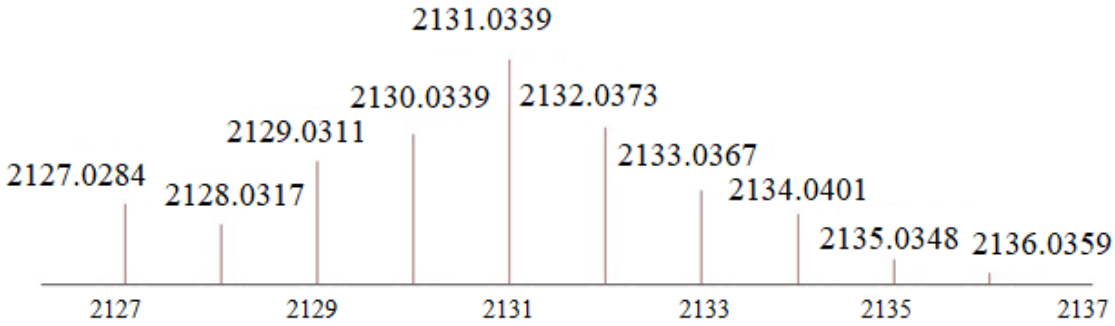


Count *vs* Mass to charge (m/z)

**Fig. S9** Experimental (top) and theoretical (bottom) isotopic distribution patterns of ESI-mass spectrum of [{$(CO)_3Re(\mu\text{-}SC_6H_4CH_3)_2Re(CO)_3\}_2(\mu\text{-}\eta^4$-ptpc)] (**2**) $[M+H]^+$.

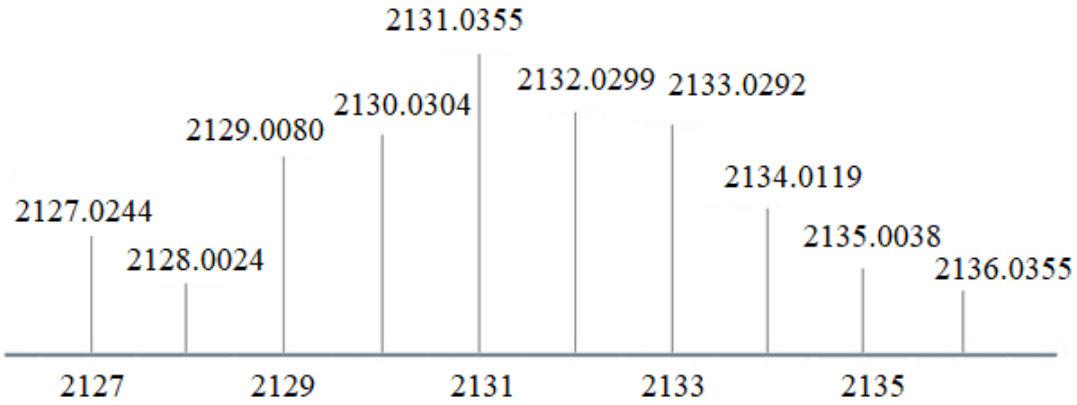


Count *vs* Mass to charge (m/z)

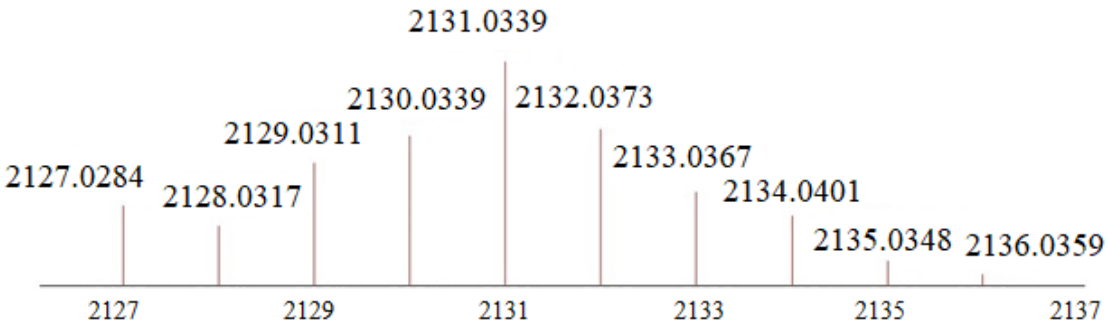


Count *vs* Mass to charge (m/z)

**Fig. S10** Experimental (top) and theoretical (bottom) isotopic distribution patterns of ESI-mass spectrum of [{$(CO)_3Re(\mu\text{-}SCH_2C_6H_5)_2Re(CO)_3$}$_2$($\mu$-$\eta^4$-ptpc)] (**3**) $[M+H]^+$.

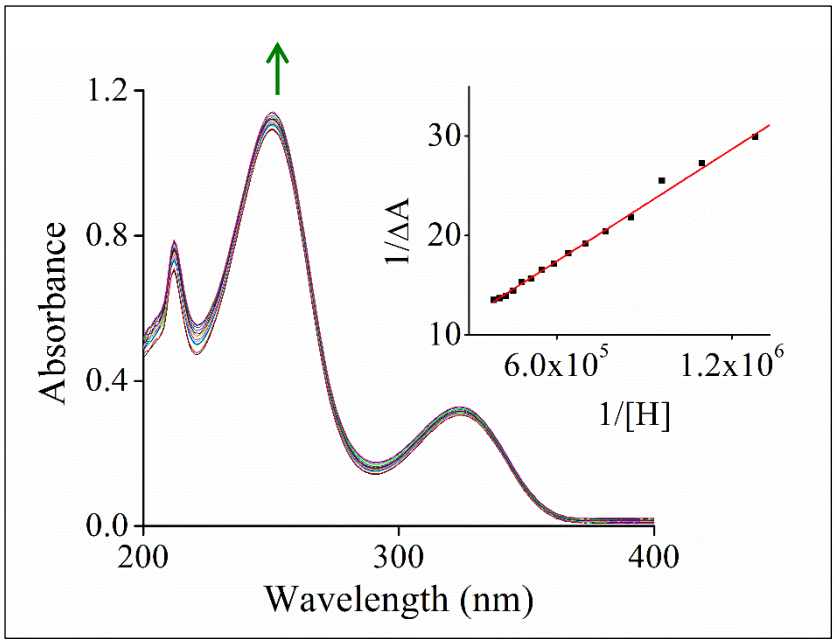


**Fig. S11** Electronic absorption spectra of *p*-phenylenediamine ($1.3\times10^{-4}$ M) increasing upon incremental addition of host **2** ($2.0–24.0\times10^{-7}$ M) in tetrahydrofuran and inset shows the corresponding Benesi-Hildebrand plot. Regression analysis was carried out at $\lambda_{max}$ 249 nm.

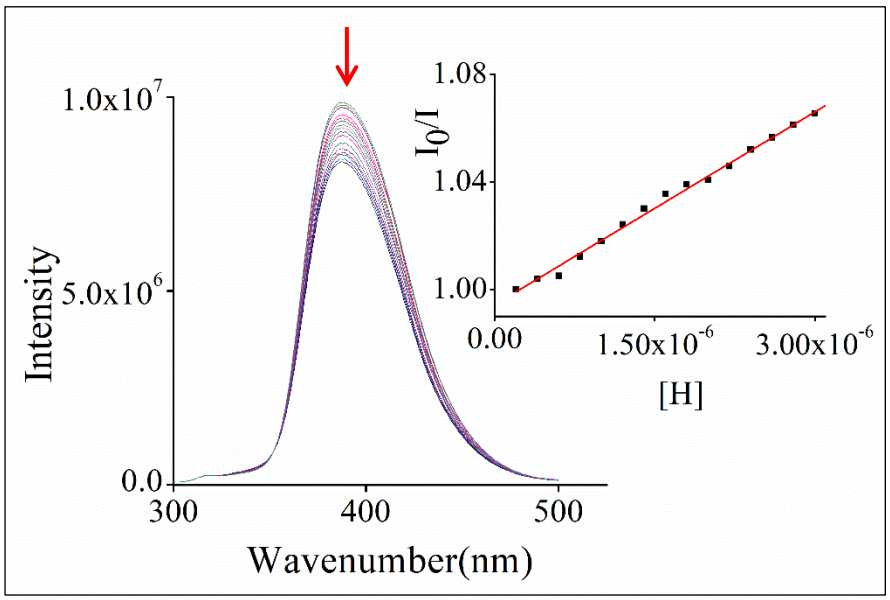


**Fig. S12** Emission intensity of *p*-phenylenediamine ($1.3\times10^{-4}$ M) decreasing with incremental addition of host **2** ($2.0–24.0\times10^{-7}$M) in tetrahydrofuran and inset shows the corresponding Stern-Volmer plot. Regression analysis was carried out at $\lambda_{max}$ 387 nm.

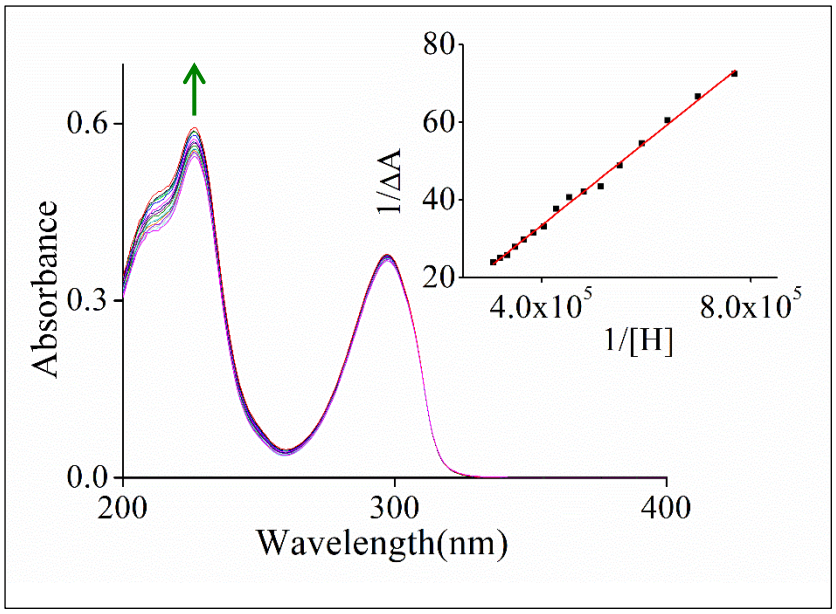


**Fig. S13** Electronic absorption spectra of quinol ($1.3\times10^{-4}$ M) increasing upon incremental addition of host **2** ($2.0–24.0\times10^{-7}$ M) in tetrahydrofuran and inset shows the corresponding Benesi-Hildebrand plot. Regression analysis was carried out at $\lambda_{max}$ 225 nm.

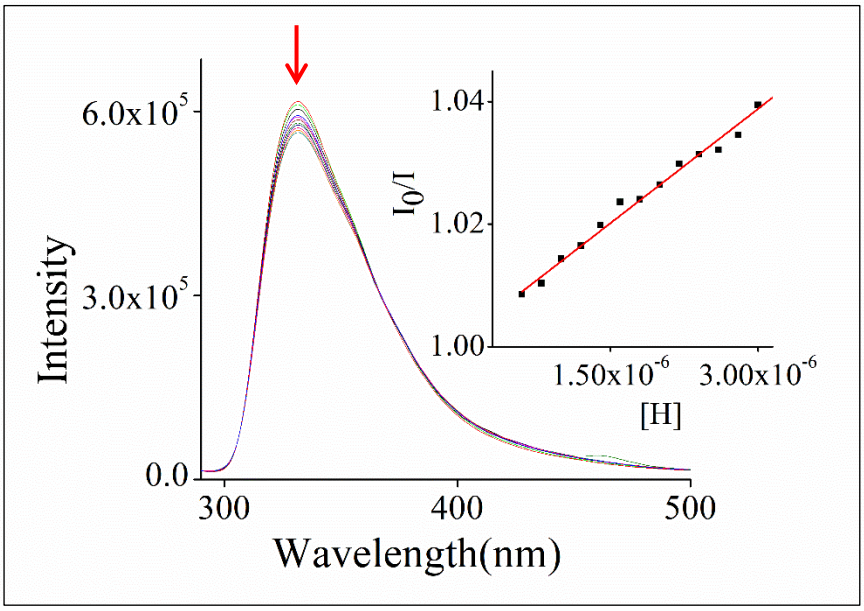


**Fig. S14** Emission intensity of quinol ($1.3\times10^{-4}$ M) decreasing with incremental addition of host **2** ($2.0–24.0\times10^{-7}$M) in tetrahydrofuran and inset shows the corresponding Stern-Volmer plot. Regression analysis was carried out at $\lambda_{max}$ 330 nm.

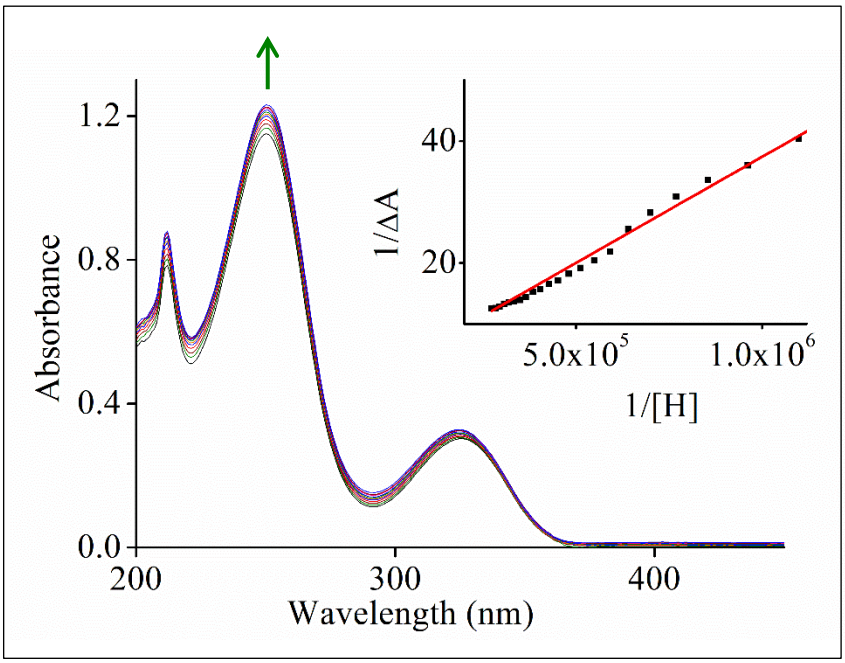


**Fig. S15** Electronic absorption spectra of *p*-phenylenediamine ($1.3\times10^{-4}$ M) increasing upon incremental addition of host **3** ($2.0–24.0\times10^{-7}$ M) in tetrahydrofuran and inset shows the corresponding Benesi-Hildebrand plot. Regression analysis was carried out at $\lambda_{max}$ 252 nm.

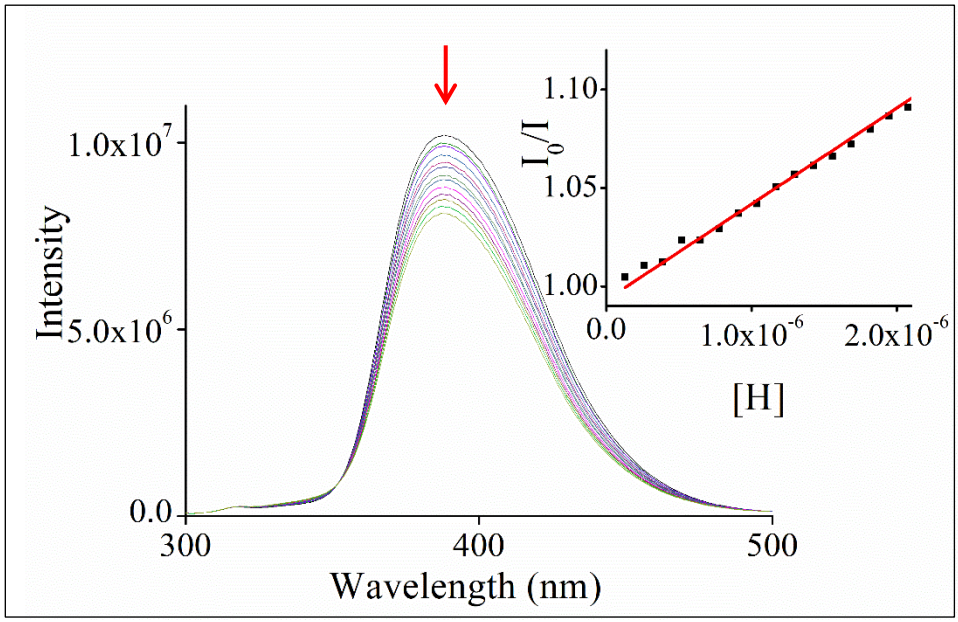


**Fig. S16** Emission intensity of *p*-phenylenediamine ($1.3\times10^{-4}$ M) decreasing with incremental addition of host **3** ($2.0–24.0\times10^{-7}$M) in tetrahydrofuran and inset shows the corresponding Stern-Volmer plot. Regression analysis was carried out at $\lambda_{max}$ 380 nm

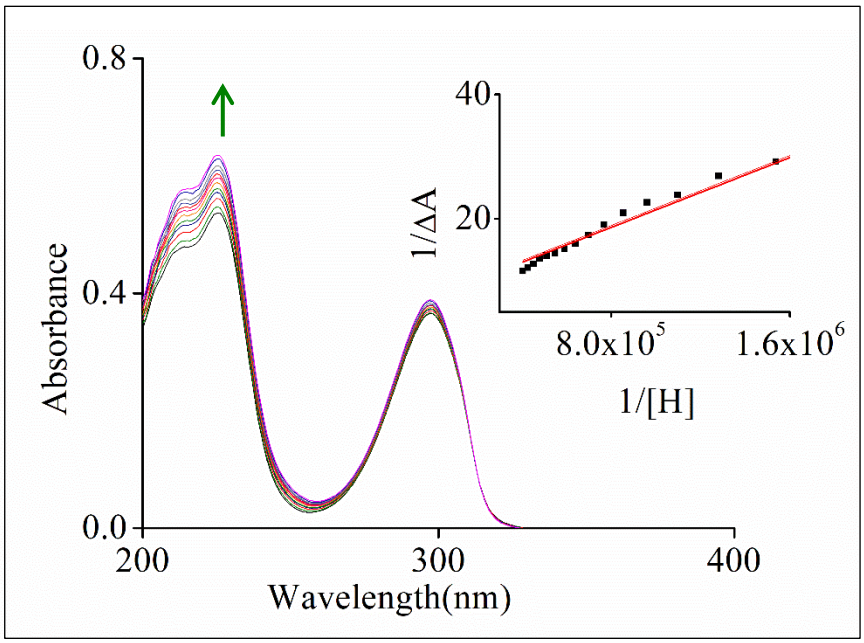


**Fig. S17** Electronic absorption spectra of quinol ($1.3\times10^{-4}$ M) increasing upon incremental addition of host **3** ($2.0–24.0\times10^{-7}$ M) in tetrahydrofuran and inset shows the corresponding Benesi-Hildebrand plot. Regression analysis was carried out at $\lambda_{max}$ 226 nm.

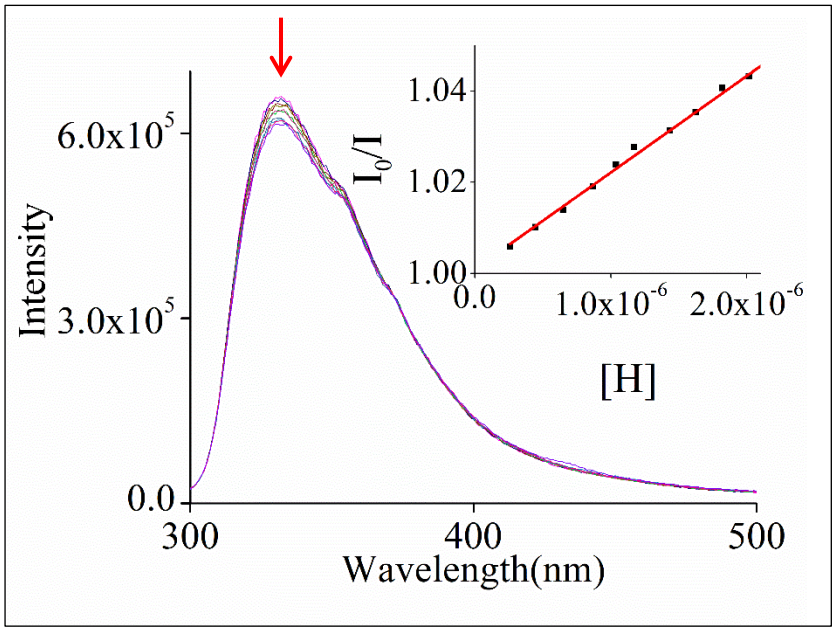


**Fig. S18** Emission intensity of quinol ($1.3\times10^{-4}$ M) decreasing with incremental addition of host **3** ($2.0–24.0\times10^{-7}$M) in tetrahydrofuran and inset shows the corresponding Stern-Volmer plot. Regression analysis was carried out at $\lambda_{max}$ 331 nm.